Journal of Materials Science and Engineering with Advanced Technology
Volume 5, Number 2, 2012, Pages 97-106

MICROSTRUCTURE AND ELECTRODE CHARACTERISTICS OF $Ti_{0.25}V_{0.34}Al_{0.01}Cr_{0.1}Ni_{0.3}$ METAL HYDRIDE ELECTRODE ALLOY

YU QING QIAO[1], MIN SHOU ZHAO[1] and LI MIN WANG[2]

[1]College of Environmental and Chemical Engineering
Yanshan University
Qinhuangdao 066004
P. R. China
e-mail: qiaoyq@ysu.edu.cn

[2]State Key Laboratory of Rare Earth Resource Utilization
Changchun Institute of Applied Chemistry
Chinese Academy of Sciences
Changchun 130022
P. R. China

Abstract

Microstructure and electrode characteristics of $Ti_{0.25}V_{0.34}Al_{0.01}Cr_{0.1}Ni_{0.3}$ metal hydride electrode alloy have been investigated by XRD, FESEM-EDS, and EIS measurements. The result shows that the alloy is mainly composed of V-based solid solution phase with body-centered-cubic structure and TiNi-based secondary phase. The discharge capacity increases with increasing temperature in a wider temperature region from 303K to 343K. The result of electrochemical impedance spectrometry indicates that the charge transfer resistance decreases with increasing temperature, while the exchange current density in the bulk of the alloy increases with increasing temperature.

Keywords and phrases: metal hydride electrode, Ni-MH batter, V-based solid solution.

Received February 23, 2012

1. Introduction

It is well known that the atomic radius and melting point of the constituent elements must be considered in solid solution alloying process. It is accepted that a large difference in the atomic radii between the matrix element and other constituent elements affects the microstructure and phase composition, and may be a key issue in forming a solid solution alloy [2, 5, 7]. In our previously work, Ce has been used as the additional element to Ti-V-Cr-Ni electrode alloy and the result showed that Ce has a great effect on the microstructure and electrochemical properties, especially on the discharge capacity and cycle stability [3, 4]. Among all the constituents, Ce has a larger atomic radius, r_{Ce}0.182nm, which is far more than that of V, r_V0.135nm, and enters in the solid solution alloy difficultly. Moreover, a large difference in the melting point (T_{Ce}1071K < T_V1900K) would result in the segregating of Ce during solidification and forming lard, which is perhaps another reason why Ce exists only in the lard. In this paper, microstructure and some dynamic parameters of $Ti_{0.25}V_{0.34}Al_{0.01}Cr_{0.1}Ni_{0.3}$ electrode alloy have been investigated.

2. Experimental

$Ti_{0.25}V_{0.34}Al_{0.01}Cr_{0.1}Ni_{0.3}$ electrode alloy is prepared by arc-melting the component metals on water cooled copper hearth under argon and re-melted for three times to ensure the homogeneity. The crystal structure of the alloy is investigated by X-ray diffraction on Rigaku D/max 2500pc X-ray diffraction meter by using JAD5 software, the microstructure and the phase compositions of the alloy are measured by FESEM-EDS analysis on XL30 ESEM FEG scanning electron microscope. The electrochemical measurements are performed in a half-cell system, and the measurement was similar to those described in our previous work [4]. To investigate the dehydriding kinetics parameters of Ti-V-Cr-Ni hydride alloy, EIS has been used for determining the charge-transfer

resistance (R_T) by using Solartron SI1187 electrochemical interface with 1255B frequency response analyzer and ZPLOT electrochemical impedance software. According to the analysis model proposed by Kuriyama et al. [1], R_T can be calculated by using least-square method, and the exchange current density (I_0) in the bulk of the alloy and the apparent energy ($\Delta_r H$) can be calculated from the following formulation (1) and (2) [6], respectively, where R, T, and F have their general meanings.

$$I_0 = RT / FR_T, \tag{1}$$

$$\lg(T / R_T) = -\Delta_r H / 2.303RT + A. \tag{2}$$

3. Results and Discussion

Figure 1 shows the XRD pattern of $Ti_{0.25}V_{0.34}Al_{0.01}Cr_{0.1}Ni_{0.3}$ electrode alloy synthesized by arc melting. It can be found that the alloy is composed of a V-based solid solution phase with body-centered-cube (bcc) structure in space group $Im3m$ and TiNi-based secondary phase. The lattice parameter and the cell volume of the bcc phase are 0.2990nm and 0.0266nm^3, respectively.

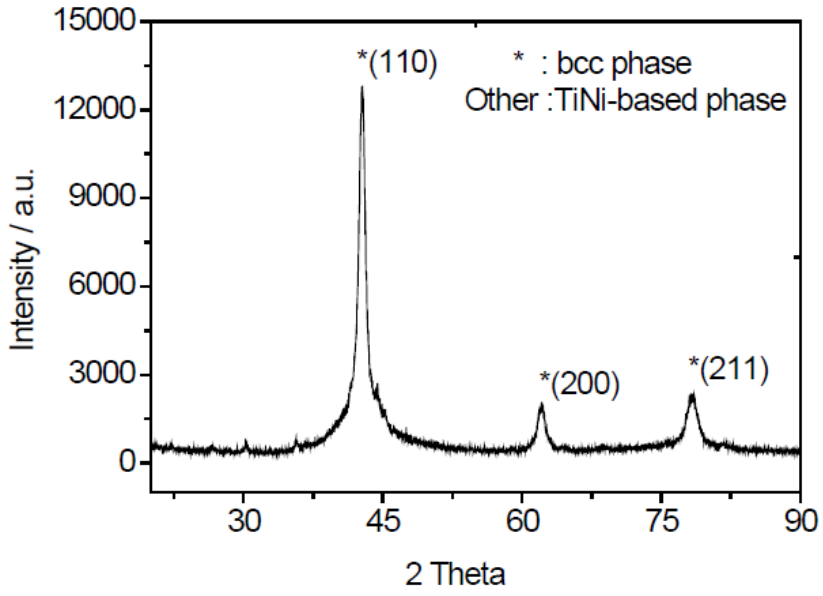

Figure 1. X-ray diffraction pattern of $Ti_{0.25}V_{0.34}Al_{0.01}Cr_{0.10}Ni_{0.30}$ electrode alloy.

Figures 2 and 3 show FESEM micrographs of $Ti_{0.25}V_{0.34}Al_{0.01}Cr_{0.1}Ni_{0.3}$ electrode alloy. It is obvious that the alloy is composed of V-based solid solution phase with dendritic shape (Figure 3) and a continuous TiNi-based secondary phase with networked shape surrounding the dendrite. The phase composition of the alloy has been semi-quantitatively analyzed with EDS, which is shown in Figure 2 and the results are shown in Table 1. It can be seen that V-based solid solution phase is mainly composed of V and Cr, while TiNi-based secondary phase is mainly composed of Ti and Ni. It is found that Al exists in all the parts of the alloy, which is difference with that of Ce.

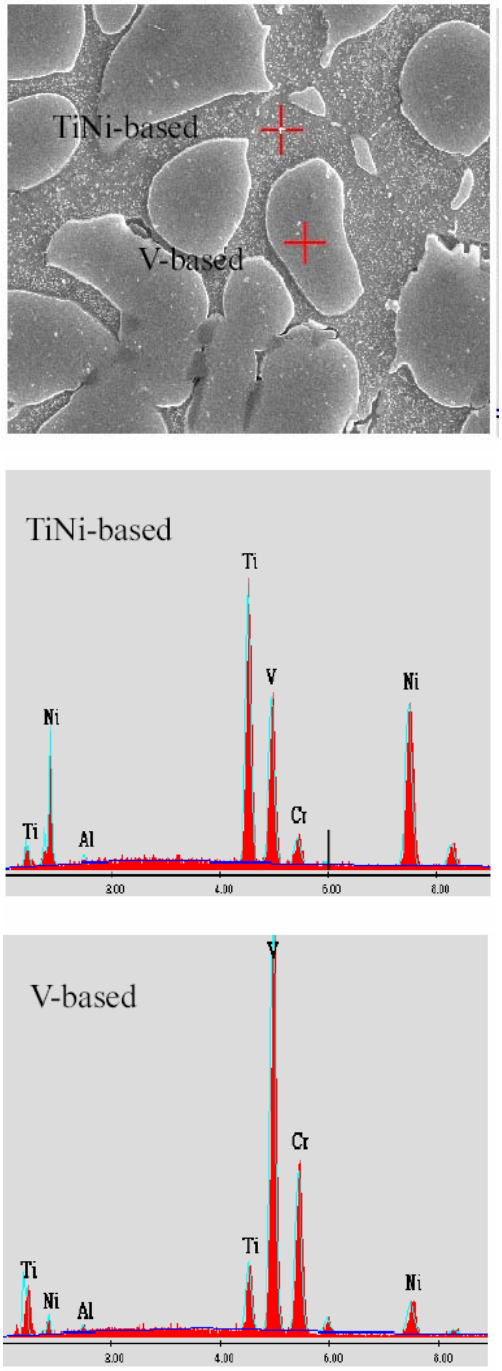

Figure 2. FESEM-EDS of $Ti_{0.25}V_{0.34}Al_{0.01}Cr_{0.10}Ni_{0.30}$ electrode alloy.

Table 1. Phase composition, lattice parameter, and cell volume of $Ti_{0.25}V_{0.34}Al_{0.01}Cr_{0.10}Ni_{0.30}$ electrode alloy

Phases	Composition (atom%)					Lattice parameter(nm)		Cell volume(nm^3)
	Ti	V	Cr	Ni	Al	a	c	
bcc phase	8.65	62.86	16.76	9.94	1.79	0.2990		0.0266
TiNi-based phase	33.72	17.68	1.76	44.75	2.10			

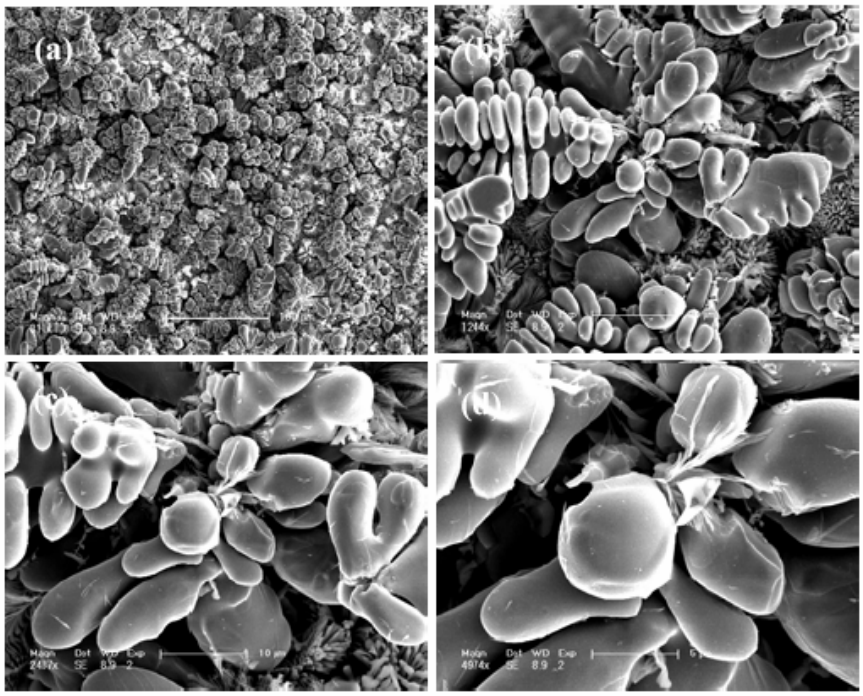

Figure 3. FESEM of bcc phase for $Ti_{0.25}V_{0.34}Al_{0.01}Cr_{0.10}Ni_{0.30}$ electrode alloy.

The cycle stability of $Ti_{0.25}V_{0.34}Al_{0.01}Cr_{0.10}Ni_{0.30}$ electrode alloy is shown in Figure 4 and the cycle stability can be described by $S_{100}(\%) = C_{100}/C_{max} \times 100$, where S_{100}, C_{100}, and C_{max} denote the

cycle stability, the discharge capacity at the 100th cycles, and the maximum discharge capacity, respectively. The result shows that the discharge capacity at 100th cycles is $216.8 mAhg^{-1}$, which is about 88.2% of the maximum discharge capacity ($245.8 mAhg^{-1}$), and implies cycle stability of the alloy electrode is acceptable. The alloy electrode containing Al is gradually activated during charge/discharge cycle process and reached the maximum discharge capacity at 10th cycles to be proved to have the lower electrochemical activity.

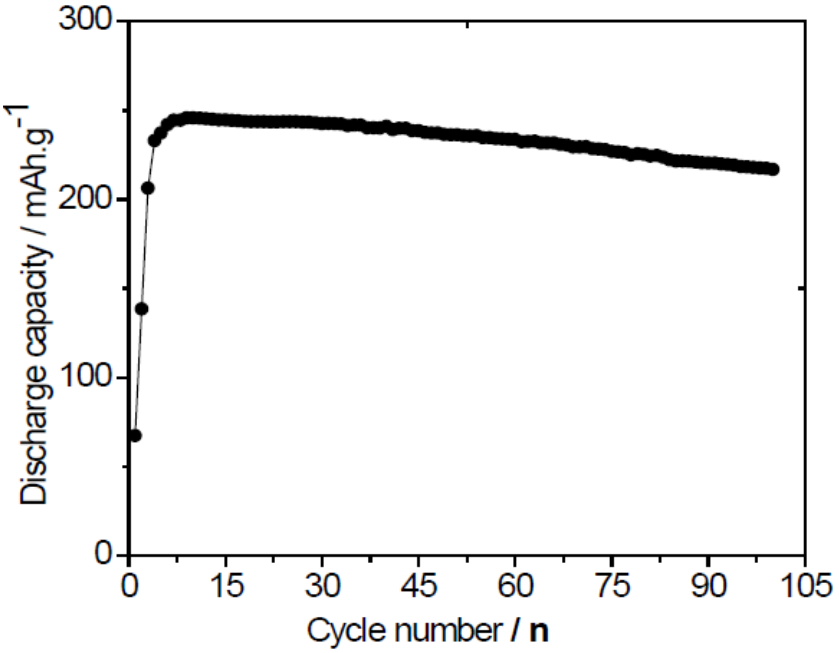

Figure 4. Discharge capacity as a function of cycle number for $Ti_{0.25}V_{0.34}Al_{0.01}Cr_{0.10}Ni_{0.30}$ electrode alloy at 303K.

Figure 5(a) shows the dependence of the discharge capacity of $Ti_{0.25}V_{0.34}Al_{0.01}Cr_{0.10}Ni_{0.30}$ electrode alloy on different temperature. For example, the discharge capacity of the alloy electrode is $258.3 mAhg^{-1}$ and $268.7 mAhg^{-1}$ at 323K and 343K, respectively. The alloy electrode

has higher discharge capacity, 245.8mAhg^{-1} ~ 268.7mAhg^{-1}, within a wide temperature region from 303K to 343K. It implies that the discharge capacity of $Ti_{0.25}V_{0.34}Al_{0.01}Cr_{0.10}Ni_{0.30}$ electrode alloy is not sensitive to temperature within the temperature span. This characteristic of the alloy is crucial for it to be used as a negative electrode material of Ni-MH batteries.

Figure 5(b) shows the effect of temperature on EIS of $Ti_{0.25}V_{0.34}Al_{0.01}Cr_{0.10}Ni_{0.30}$ electrode alloy in the 50^{th} cycles at 50% DOD. It is obvious that temperature has a great effect on the radii of the semi-circles in low-frequency region, which decreases with increasing temperature markedly. Part of the fitting results of R_T and the calculated I_0 are summarized in Table 2. It is found that R_T decreases with increasing temperature, which is 3.703Ω, 0.595Ω, and 0.301Ω at 303K, 323K, and 343K, respectively. However, I_0 increases with increasing temperature, which is 84.30mAg^{-1}, 311.95mAg^{-1}, and 654.51mAg^{-1} at 303K, 323K, and 343K, respectively.

Figure 5(c) shows the semi-logarithmic plot of charge transfer resistance to reciprocal temperature $(1/T)$ for $Ti_{0.25}V_{0.34}Al_{0.01}Cr_{0.10}Ni_{0.30}$ electrode alloy. It can be seen that the plot follows a linear dependence, which accords with Arrhenius relationship and coincides with that presented by Liu et al. [2]. The activation energy $(\Delta_r H)$ for charge-transfer reaction is calculated from: $\lg(T/R_T) = -\Delta_r H/2.303RT + A$, the result shows that the activation energy for charge-transfer reaction is 55.7KJmol^{-1} and larger than that on $MINi_{3.75}Co_{0.65}Mn_{0.4}Al_{0.2}$ hydrogen storage alloy, $28.1\ \text{KJ mol}^{-1}$ (Ml = La-rich mischmetal) [6]. The electrochemical activity of the alloy seems to be poor comparing with AB_5 type alloy.

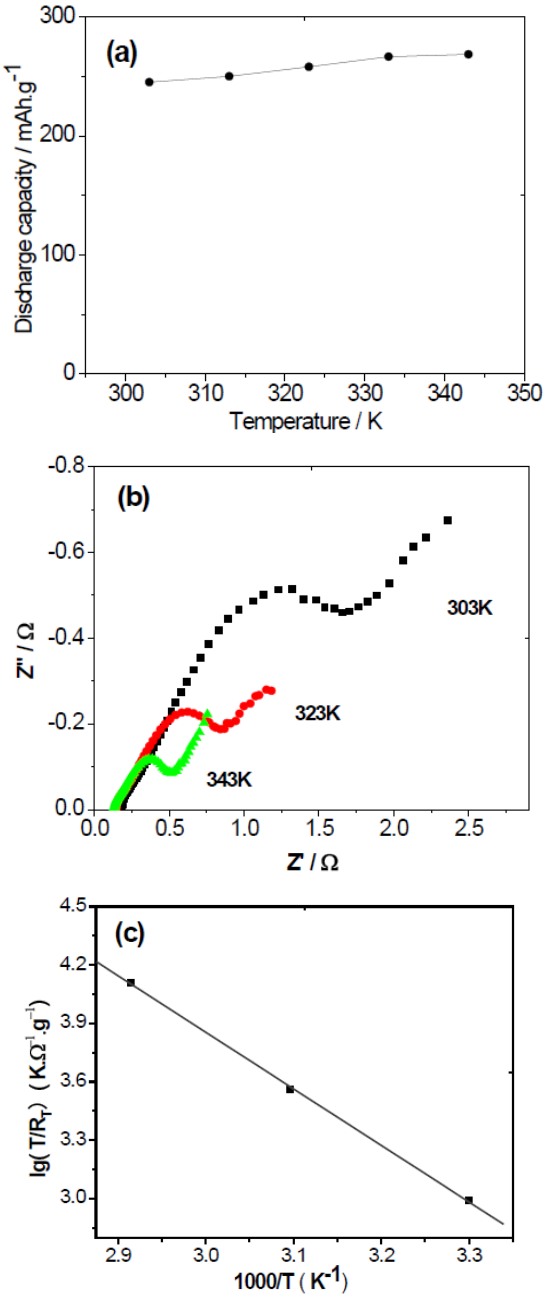

Figure 5. (a) Effect of temperature on discharge capacity, (b) electrochemical impedance spectroscopy, and (c) $\lg(T/R_T)$ with $1/T$ at 50 DOD for $Ti_{0.25}V_{0.34}Al_{0.01}Cr_{0.10}Ni_{0.30}$ electrode alloy.

Table 2. Some dynamic parameters of $Ti_{0.25}V_{0.34}Al_{0.01}Cr_{0.1}Ni_{0.3}$ electrode alloy

Temperature(K)	$R_T(\Omega)$	I_0(mA / g)	C_{max}(mAh / g)
303	3.703	84.30	245.8
323	0.595	311.95	258.3
343	0.301	654.51	268.7

Acknowledgement

This work was financially supported by the Foundation of He'bei Educational Committee (Z2010337), Soft Science Project of Hebei Province Science and Research Foundation (11457298), and Doctoral Foundation of Yanshan University (No. B330).

References

[1] N. Kuriyama, T. Sakai and H. Miyamura et al., J. Alloys Compds. 202 (1993), 183.

[2] Y. F. Liu, H. G. Pan and M. X. Gao et al., Electrochimica Acta 49 (2004), 545.

[3] Y. Q. Qiao, M. S. Zhao and M. Y. Li et al., Scripta Materialia 55 (2006), 279.

[4] Y. Q. Qiao, M. S. Zhao and X. J. Zhu et al., J. Rare Earths 25 (2007), 341.

[5] M. Tsukahara, K. Tskahasha and T. Mishima et al., J. Alloys Compds. 243 (1996), 133.

[6] X. X. Yuan and N. X. Xu, Acta Chimica Sinica 60 (2002), 13.

[7] Q. A. Zhang, Y. Q. Lei and L. X. Chen, Mater. Chem. Phys. 71 (2001), 58.

■